Quantum Transport in Nanotube Transistors

François Léonard

Sandia National Laboratories,
MS 9161, Livermore, CA 94551, USA, fleonar@ca.sandia.gov

ABSTRACT

We discuss recent calculations of electronic transport in a 10 nm long, three-terminal carbon nanotube device. By calculating self-consistently the electrostatic potential and charge in the device, we obtain the band bending along the nanotube as a function of the applied voltages. This band bending strongly influences the transmission of carriers across the nanotube, giving rise to "on" and "off" regimes characteristic of transistor action. Hence,

keywords: nanotube, electronic transport, transistor, ballistic, nanowire

1. INTRODUCTION

Recently, much work has focused on novel electronic materials to replace conventional silicon-based electronics. In particular, materials that could function at nanoscale dimensions are much sought, with their promise of greater device densities. Carbon nanotubes (NTs) [1] are potential candidates due to their unique electronic and mechanical properties. Three-terminal NT devices using NTs as the transport channel have already been fabricated in the laboratory by a number of groups [2–5], and have demonstrated desirable functionality such as transistor action. Such experimental observations pose a number of challenges to theory, from fundamental to more applied perspectives [6–15]. Understanding these issues is crucial if NTs are to become more prominent technologically.

The present paper describes our recent efforts to theoretically address the issue of how a NT transistor works. For this purpose, one needs to understand how current flows across the NT transistor, and what factors influence this current flow. Our method to study electronic transport in NT transistors combines a self-consistent procedure for the electrostatics with a quantum transport calculation, allowing us to calculate, for example, the conductance of a NT transistor as a function of the gate voltage. We show that a simple device using a single-wall, semiconducting NT, can function as a conventional transistor, with "on" and "off" states that can be controlled by an applied gate voltage. The calculations are performed for a 10 nm long device, illustrating that nanotube devices should perform extremelly well even at reduced dimensions.

2. MODEL

The geometry of our model NT transistor is shown in Fig. 1. It consists of a single-wall, semiconducting NT embedded in metal at its two ends. These metals serve as the source and drain contacts to the NT. In the central portion of the device, the NT is embedded in a cylindrical dielectric material (dielectric constant $\varepsilon = 3.9$) of radius 10 nm. A cylindrical gate wraps the dielectric and the voltage applied to this terminal serves to control the behavior of the device. Here, we make the assumption that the NT interacts with the metals and the dielectric only through van der Waals interactions, so the NT is separated from the metals and the dielectric by a vaccuum gap of 0.3 nm, characteristic of van der Waals interactions. The metal Fermi level is chosen to be 1 eV below the NT midgap, which is typical of metals used experimentally.

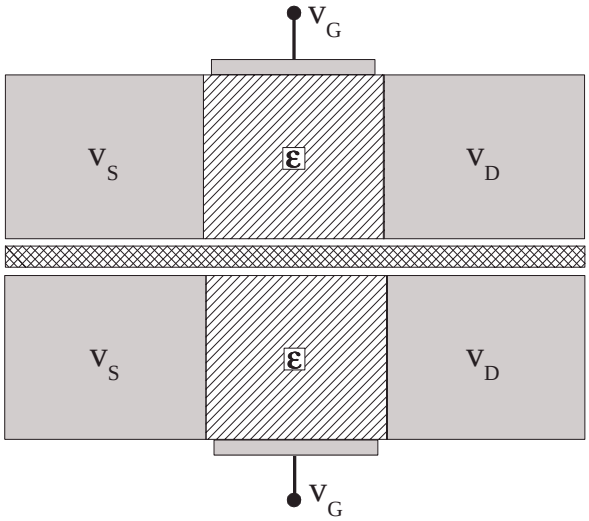

FIG. 1. Cross-sections of the nanotube device. Gray areas are the gate and the metallic source and drain contacts to the nanotube. Hatched areas represent the dielectric that surrounds the nanotube, and cross-hatched area is the nanotube. Source-drain separation is 10 nm; cylindrical gate has a radius of 10 nm. The separation between the nanotube and the metals or the dielectric is 0.3 nm.

While the general behavior of the device is unaffected by the precise NT used (as long as it is semiconducting and has a reasonable band-gap), we choose a specific NT to make the calculations explicit. Experiments typically use NTs with band-gaps of about 0.5 eV; and the simplest NT geometry to treat computationally is that of

zigzag tubes. So, for our calculations, we choose a (17,0) zigzag NT, which has a radius of 0.66 nm and a band gap of 0.55 eV within the tight-binding model discussed below. Structurally, a (n,0) zigzag NT can be viewed as parallel rings of n atoms alternately spaced by 0.14 nm and 0.07 nm.

Our general method to compute the conductance across the NT device is illustrated in Fig. 2. In order to calculate the conductance, the transmission probability of electrons at a given energy $T(E)$ must be determined for the electrostatic potential present along the NT. So the first part in the calculation is to self-consistently obtain Φ and the charge density ρ in the device.

The initial step in the procedure consists of specifying the device geometry, material parameters and applied voltages. We then begin the calculational part of the procedure by making an initial guess for ρ. The electrostatic potential is then calculated by solving Poisson's equation with boundary conditions at the metal and dielectric surfaces.

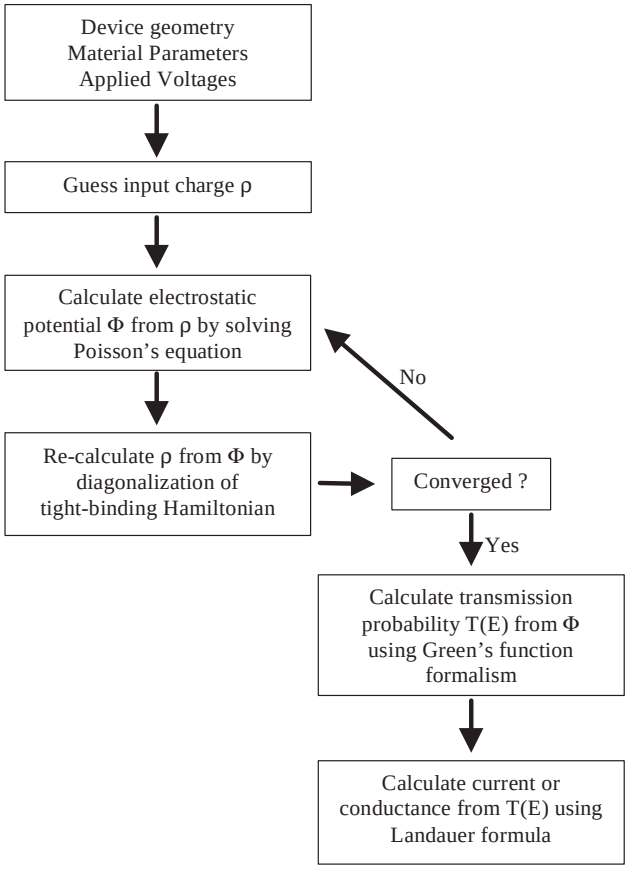

FIG. 2. Flow chart of the computational procedure to calculate the device conductance. See text for details.

The next step in the procedure is to calculate the charge ρ from the freshly calculated Φ. To obtain ρ, we proceed within a tight binding approximation with one π orbital per carbon atom. The Hamiltonian for a (n,0) zigzag tube N rings long is written as

$$H = \begin{bmatrix} -e\Phi(z_1) & A & 0 & 0 & 0 & 0 & B \\ A & -e\Phi(z_2) & B & 0 & 0 & 0 & 0 \\ 0 & B & -e\Phi(z_3) & A & 0 & 0 & 0 \\ 0 & 0 & \bullet & \bullet & \bullet & 0 & 0 \\ 0 & 0 & 0 & \bullet & \bullet & \bullet & 0 \\ 0 & 0 & 0 & 0 & \bullet & \bullet & \bullet \\ B & 0 & 0 & 0 & 0 & A & -e\Phi(z_N) \end{bmatrix} \quad (1)$$

with $A = 2n\gamma_0 \cos\left(\frac{\pi J}{n}\right)$, $B = n\gamma_0$ and periodic boundary conditions. Here, the subscript i on z_i refers to the ith ring along the tube axis. γ_0 is the nearest-neighbor matrix element, taken as 2.5 eV here, and $J = 1, ..., n$ represents the Jth band originating from quantization of the circumferential wavevector. Diagonalization of the Hamiltonian yields the coefficients of the wavefunctions on each of the rings, as well as their energy. The coefficients only give the total charge on a ring, so to get the spatial distribution $\rho(r, z)$, we smear the total charge over a length 0.07 nm of the NT cylinder and over a radial thickness of 0.1 nm.

The above procedure is repeated until we obtain a self-consistent solution for ρ and Φ. Once this is completed, we then proceed to the second part of the calculation, which is to calculate the transmission probability across the device as a function of energy. This is done using a Green's function formalism [16]. To implement this formalism, the NT device is divided into three regions: two semi-infinite "leads", and a "device region", which is 18.3 nm in length here. Within the scattering region we use the full self-consistent potential $\Phi(z)$. The potentials in the leads are taken as constant, and equal to the potentials at the boundaries of the scattering region. The transmission probability $T(E)$ is given by

$$T(E) = Tr(\Gamma_L G^r \Gamma_R G^a) \quad (2)$$

where Γ_L and Γ_R couple the device to the left and right leads, while G^r and G^a are the retarded and advanced Green's functions for the device. The Green's function is calculated by solving

$$\left(EI - H - \Sigma_L^r - \Sigma_R^r\right) G^r = I \quad (3)$$

where H is given in Eq. (1) and includes the self-consistent electrostatic potential Φ. Σ_L^r and Σ_R^r are self-energies due to the semi-infinite left and right leads. The coupling matrices Γ_L and Γ_R are related to the self-energies through

$$\Gamma_{L,R} = -2\,\mathrm{Im}\left(\Sigma_{L,R}^r\right). \quad (4)$$

The self-energies are related to the Green's function of the semi-infinite leads through

$$\Sigma_{L,R}^r = \tau_{L,R}^\dagger g_{L,R}^r \tau_{L,R} \quad (5)$$

where $g_{L,R}^r$ is the Green's function of the left and right semi-infinite lead, and $\tau_{L,R}$ is a matrix that couples the

device to the leads. Since only the first and last points of the device region couple to the leads, the only non-zero element of τ_L^{ij} is τ_L^{11}, while the only non-zero element of τ_R^{ij} is τ_R^{NN}. Hence, the only non-zero elements of the self-energy functions are

$$[\Sigma_L^r]_{11} = (n\gamma_0)^2 [g_L^r]_{11} \tag{6}$$

and

$$[\Sigma_R^r]_{NN} = (n\gamma_0)^2 [g_R^r]_{NN} \tag{7}$$

where we have used $\tau_L^{11} = \tau_R^{NN} = n\gamma_0$ for our zigzag NT. To solve for $[g_L^r]_{11}$ and $[g_R^r]_{NN}$, we note that the Green's functions of the semi-infinite leads also satisfy Eq. (3) :

$$\left(EI - H - \tau_L^\dagger g_{L,R}^r \tau_L - \tau_R^\dagger g_{L,R}^r \tau_R\right) g_{L,R}^r = I. \tag{8}$$

This allows us to solve for $[g_L^r]_{11}$ and $[g_R^r]_{NN}$.

Equation (2) for the transmission can be written as

$$T(E) = 4\,(n\gamma_0)^4 [g_L^r]_{11} [g_R^r]_{NN} |G_{1N}^r|^2, \tag{9}$$

so that we only need to calculate G_{1N}^r.

For a given self-consistent potential $\Phi(z)$ and energy E, we first compute $[g_L^r]_{11}$ and $[g_R^r]_{NN}$; we then obtain $[\Sigma_L^r]_{11}$ and $[\Sigma_R^r]_{NN}$ from Eq. (6) and Eq. (7). These are then used to solve the Green's function equation (3) for G_{1N}^r. Putting all of this together in Eq. (9) yields the transmission probability at energy E for a given self-consistent potential. In principle, the transmission function will have contributions from each band J; but for the present calculation, only the edge bands make significant contributions to the final conductance; furthermore, because our model device has cylindrical symmetry, there is no scattering between bands with different symmetry. So in practice, $T(E)$ is calculated only for $J = 6$.

Once the transmission function is obtained, we calculate the zero-bias conductance using the Landauer formula [16]

$$G = \frac{4e^2}{h} \int T(E) \left[-\frac{\partial f(E)}{\partial E}\right] \tag{10}$$

where the energy E is relative to the Fermi level and $f(E)$ is the Fermi function.

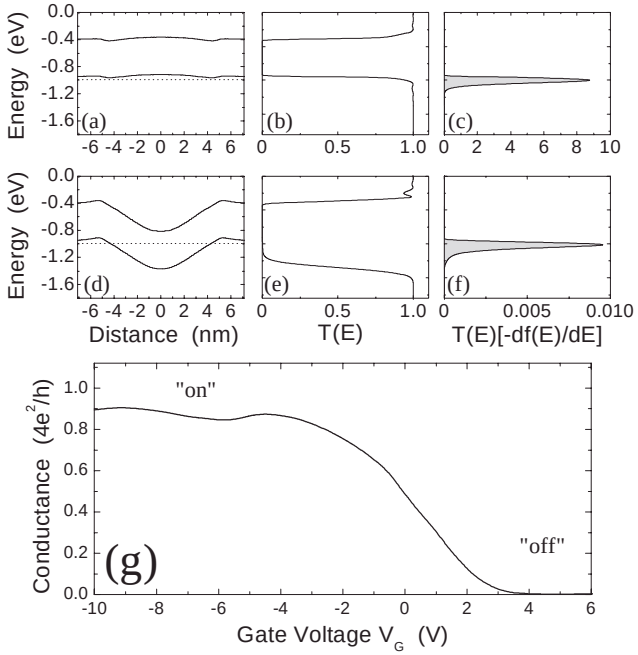

FIG. 3. (a) Local valence and conduction band edges, from the self-consistent electrostatic potential, for $V_G = -5$ V, at room temperature. Dotted line is Fermi level. (b) Transmission probability for the band-bending in (a). (c) Integrand of Eq. (10) vs energy at room temperature. Panels (d-f) is the same sequence but for $V_G = 5$ V. Note the different horizontal scales in (c) and (f). (g) Conductance of the nanotube device at low bias as a function of the gate voltage.

3. RESULTS

Figure 3(a) shows the zero-bias, self-consistent band-bending calculated for a gate voltage $V_G = -5$ V, at room temperature. Initially, the metal Fermi level is 0.725 eV below the valence band edge; but charge transfer between the metal and the NT repositions the Fermi level only 0.055 eV below the valence band edge in the contacts; this leads to hole doping of the NT. At this gate voltage, the electrostatics are such that the bands are essentially flat; this means that for energies outside the band-gap, electrons are unscattered by the potential and the transmission probability is essentially 1 [Fig. 2(b)]. Multiplying the transmission probability by the derivative of the Fermi function to yield the integrand of Eq. (10) shows that the conductance is governed by electrons in a narrow energy range of order kT around the Fermi level. Because the transmission probability at the Fermi level is high, $T(E_F) = 0.94$, the total conductance is high as shown in Fig. 2(g). (The highest conductance possible is 1 on this scale, corresponding to perfect transmission through the device.). This high conductance regime defines the "on" state of the device.

Upon an increase of the gate voltage to $V_G = 5$ V, the qualitative shape of the band-bending changes, Fig. 2(d). There is now a substantial barrier in the center of the

device, blocking the transport of electrons. For example, electrons at the Fermi level would have to tunnel through more than 8 nm of the NT in order to make it across the device. As shown in Fig. 2(e) the probability of this occurring is very low, as $T(E_F) \approx 10^{-3}$. This is further illustrated in Fig. 2(f), where the peak at the Fermi level is 3 orders of magnitube less than it was in Fig. 2(c) [note the different scales on the horizontal axis]. Hence the conductance of the device is much smaller than in the "on" regime [Fig. 2(g)] and the device has been switched "off".

4. CONCLUSION

The device discussed here behaves much like a conventional Field-Effect Transistor (FET), with "on" and "off" states that can be controlled by the gate voltage. However, the mechanisms that govern the NT transistor operation are quite different from those in conventional FETs. For example, conventional FETs rely heavily on doping to create the necessary conditions for the device to operate. In contrast, the NT transistor studied here does not require doping of the NT. Furthermore, current saturation in conventional FETs arises due to "pinch-off" effects; these issues do not apply to the NT device. Current saturation also arises in the NT device [17], but for an entirely different reason: at high bias, the current is eventually limited by the number of available carriers for transport. We have also discovered [17] additional functionality in the NT device: by driving the channel into inversion, an electrostatically defined quantum dot is created, and the NT behaves as a gated resonant-tunneling device. Such developments in the fundamental understanding of electronic transport coupled with progress in synthesis may very well lead to future technological applications.

ACKNOWLEDGEMENTS

Support from the Office of Basic Energy Sciences, Division of Materials Sciences, U.S. Department of Energy under contract No. DE-AC04-94AL85000 is acknowledged. J. Tersoff contributed to this work.

[1] C. Dekker, *Physics Today* **5**, 22 (1999).
[2] S. J. Tans, A. R. M. Verschueren, and C. Dekker, *Nature* **393**, 49 (1998).
[3] R. Martel *et al.*, *Appl. Phys. Lett.* **73**, 2447 (1998).
[4] C. Zhou, J. Kong, and H. Dai, *Appl. Phys. Lett.* **76**, 1597 (2000).
[5] K. Tsukagoshi, B. W. Alphenaar, and H. Ago, *Nature* **401**, 572 (1999).
[6] F. Léonard and J. Tersoff, *Phys. Rev. Lett.* **83**, 5174 (1999).
[7] F. Léonard and J. Tersoff, *Phys. Rev. Lett.* **84**, 4693 (2000).
[8] F. Léonard and J. Tersoff, *Phys. Rev. Lett.* **85**, 4767 (2000).
[9] M. P. Anantram, *Appl. Phys. Lett.* **78**, 2055 (2001).
[10] M. P. Anantram, S. Datta, and Y. Q. Xue, *Phys. Rev. B* **61**, 14219 (2000).
[11] M. P. Anantram and T. R. Godivan, Phys. *Rev. B* **58**, 4882 (1998).
[12] K. Esfarjani, A.A. Farajian, and Y. Kawazoe, *Appl. Phys. Lett.* **74**, 79 (1999).
[13] A. Odintsov, *Phys. Rev. Lett.* **85**, 150 (2000).
[14] A. S. Maksimenko and G. Y. Slepyan, *Phys. Rev. Lett.* **84**, 362 (2000).
[15] H. Mehrez *et al.*, *Phys. Rev. Lett.* **84**, 2682 (2000).
[16] S. Datta, *Electronic transport in mesoscopic systems* (Cambridge University Press, Cambridge, 1995).
[17] F. Léonard and J. Tersoff, submitted.